

Appendix F: Changes in Vulnerability to Lateral Spreading

F1 Introduction

In parts of Christchurch in close proximity to streams and rivers the four main earthquakes in the Canterbury Earthquake Sequence (**CES**) caused extensive liquefaction related lateral spreading. This lateral spreading resulted in significant damage to buildings, bridges, underground services and roads. The severity and extent of liquefaction related lateral spreading varied for each main earthquake in the CES.

Figure F1.1 presents the lateral spreading observations and free field liquefaction observations (i.e. flat land away from the influence of rivers and streams) recorded over the four main earthquakes during the CES.

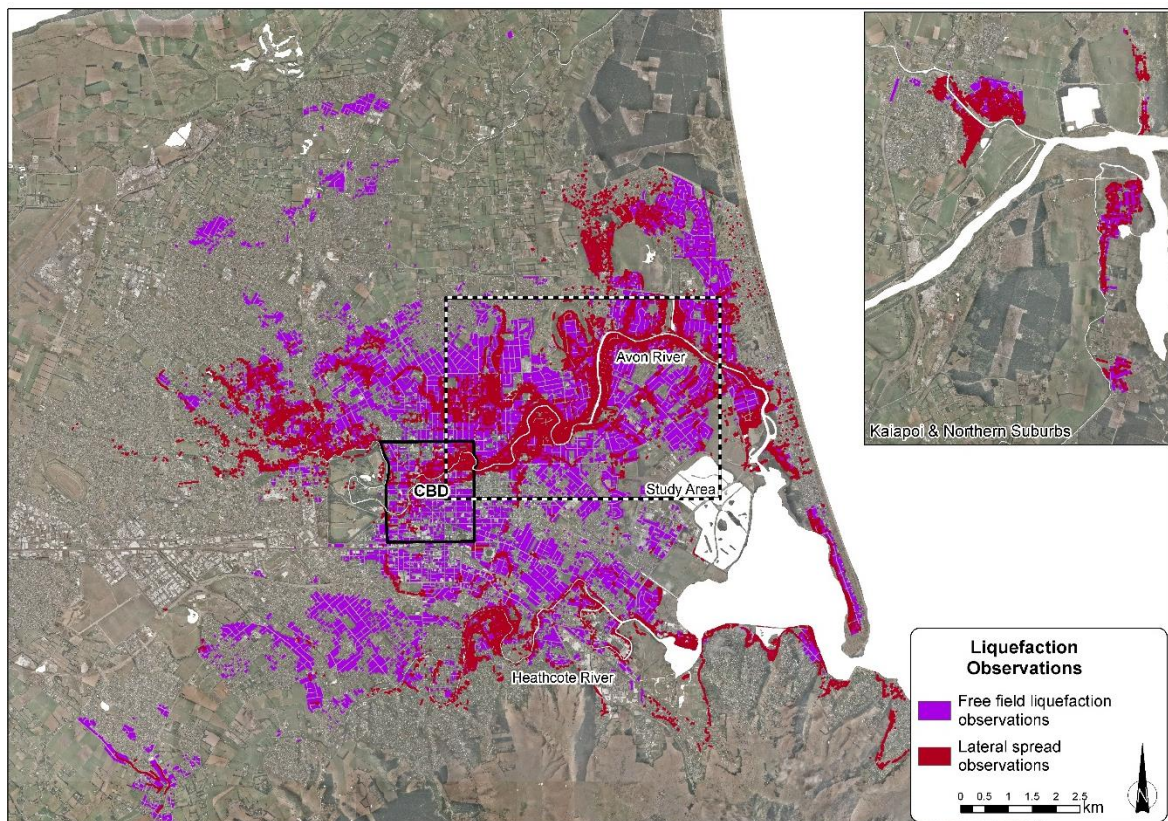


Figure F1.1: Lateral spreading and free field liquefaction observations during the CES. The lateral spreading observations shown include recorded ground cracks¹ and observations of lateral spreading on residential properties². Free field liquefaction observations shown are based on land damage observations on residential properties².

Figure F1.1 shows that the majority of the lateral spreading observations were in close proximity to the rivers and streams in the Christchurch area, in particular:

- The Avon River and its tributaries which flow from west to east generally in the north eastern area of the Central Business District (**CBD**); and

¹ Observations of ground cracking in some areas is attributable to mechanisms other than lateral spreading such as ground oscillation damage.

² The land damage observations were undertaken on behalf of the EQC for the purpose of settling land damage claims on residential properties. As such the non-residential land damage was not comprehensively mapped. Hence, there are non-residential areas where lateral spreading and free field liquefaction occurred that are not presented on this figure.

- The Heathcote River which flows from west to east at the foothills of the Port Hills to the south of CBD.

Kaiapoi and the northern suburbs were also significantly affected by liquefaction related lateral spreading. The majority of the lateral spreading in Kaiapoi and the northern suburbs occurred during the September 2010 earthquake, where the seismic demand was higher compared with the subsequent CES earthquakes.

F1.1 Purpose and Outline

This appendix provides a review of lateral spreading prediction methods commonly used by engineering practitioners in New Zealand and also presents observations of lateral spreading which occurred during the CES. It demonstrates that the potential for lateral spreading in the Christchurch area very likely has not increased as a result of the physical changes to the land that occurred as a result of the CES. This conclusion forms the basis of a key assumption in the ILV Assessment Methodology, which is discussed in Section 6.6.

The ILV Assessment Methodology does not incorporate lateral spreading vulnerability into the assessment of *Criterion 1* on the basis that this type of liquefaction vulnerability very likely has not increased. Therefore, land that is unlikely to be vulnerable to free field liquefaction related damage but is vulnerable to liquefaction related lateral spreading damage does not satisfy *Criterion 1* and hence, does not qualify for ILV land damage as discussed in Section 8.4.

This appendix is structured as follows:

- Section F2 provides background information about lateral spreading including a description of the process and a summary of the measurements and observations of liquefaction related lateral spreading as a result of the CES;
- Section F3 discusses the effect of the physical changes to the land as a result of the CES on the future vulnerability to liquefaction related lateral spreading in the Christchurch area. This is discussed with reference to commonly used lateral spreading prediction models. Analyses of horizontal movements estimated from lateral spreading crack measurement observations for each earthquake as well as the LiDAR surveys demonstrates that the severity of lateral spreading likely reduced in the latter earthquakes during the CES relative to the seismic demand of each earthquake; and
- Section F4 summarises the main conclusions from this appendix.

F2 Background to Lateral Spreading

F2.1 Liquefaction Related Lateral Spreading Process

In areas with soils that are susceptible to liquefaction, significant damage to structures and lifelines can be caused by liquefaction related lateral spreading and lateral stretching (as observed in such areas through the CES). Lateral spreading occurs in areas with gentle slopes or areas with nearly level ground with a free-face in close proximity (such as a road cutting, old river terrace or river bank).

For the purposes of this appendix, lateral spreading is defined as the horizontal movement of ground towards the free-face or downslope as a result of the liquefaction of shallow underlying soil deposits. Liquefaction primarily occurs as a result of earthquake shaking of loose sands and soils. The liquefaction process and the methods used to assess liquefaction triggering and vulnerability are discussed in detail in **Appendix A**.

The schematic diagram presented in Figure F2.1 is a three dimensional depiction of liquefaction related lateral spreading. Typically, liquefaction related lateral spreading occurs at a site underlain

by liquefying soil material when either the ground is sloping or when the land is flat and in close proximity to a free-face. In the Christchurch area where the land is relatively flat and incised by river and stream channels, lateral spread areas associated with flat land and a free-face was predominant during the CES and caused severe land, infrastructure and building damage.

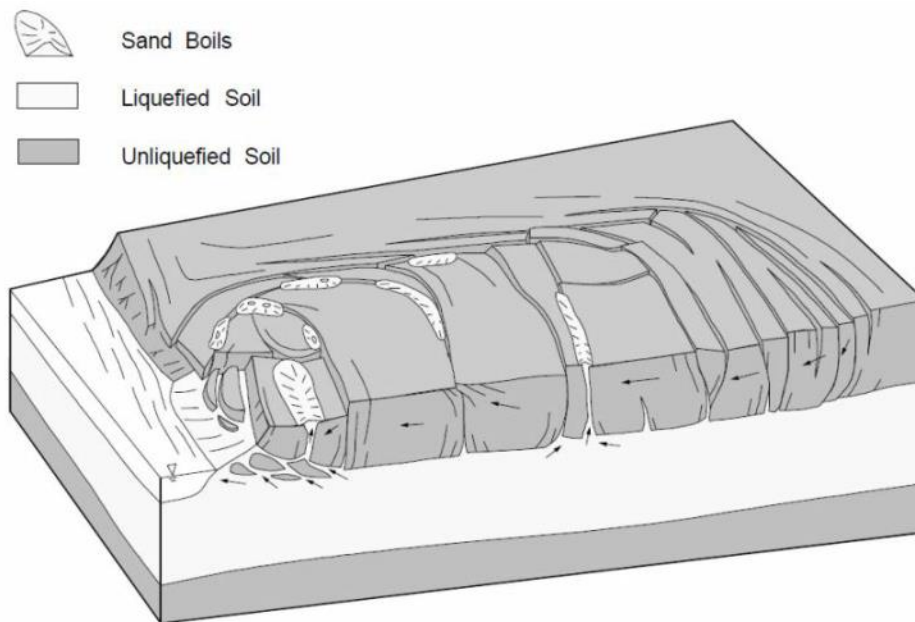


Figure F2.1: Schematic of liquefaction related lateral spreading (Deterling (2015), originally from Varnes 1978).

There is an important distinction between lateral *spreading* and lateral *stretching* as they are referred to in this appendix. Lateral stretch (also referred to as lateral strain) is a measure of the difference between the horizontal movement of two observation points over a given length, whereas lateral spread is a measure of the global horizontal movement of a block of land.

Figure F2.2 demonstrates these two concepts. Dwelling A has laterally spread on average 0.5m but it has not sustained lateral stretch across the building footprint. Dwelling B has laterally spread on average 2.25m and sustained 0.5m of lateral stretch across the building footprint.

Ground cracks are typically a manifestation of lateral stretching and occur when a block of land sustains less global horizontal movement relative to the block in front of it. It is important to note that lateral stretch is typically non-uniform, generally resulting in an irregular crack pattern. Also, the ground cracks are not always visible at the ground surface.

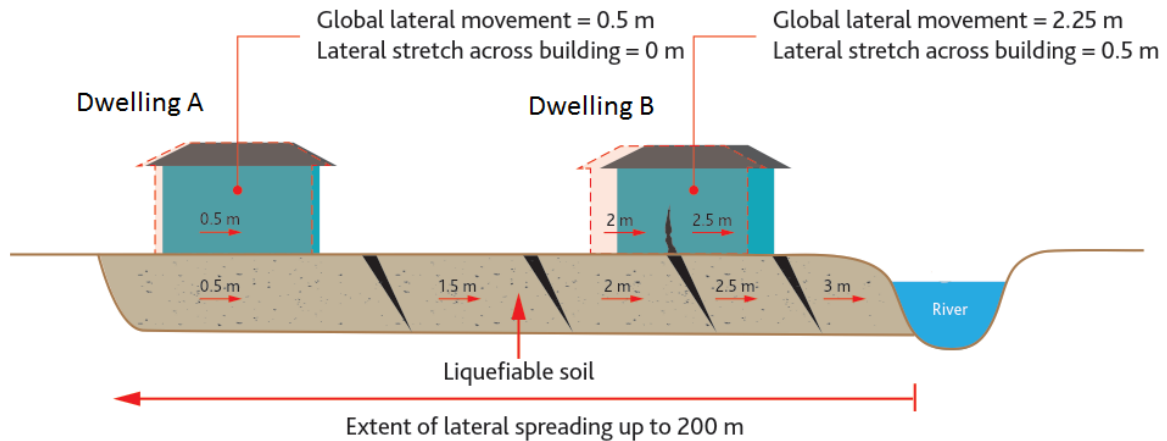


Figure F2.2: Simplified cross-section showing large-scale lateral spreading and localised lateral stretching of gently-sloping land.

F2.2 Lateral Spreading during the CES

The white and black dashed box in Figure F1.1 indicates the study area that is the focus of this appendix. This study area has been chosen because it covers the general areas in Christchurch with the most severe and extensive liquefaction related lateral spreading. Figure F2.3 is an expanded view of this study area showing the ground surface elevation prior to the CES with estimated horizontal movement vectors derived from LiDAR survey data overlaid. Large arrows indicating the general direction of significant horizontal movements are shown. This figure also shows the river cross-section locations that are discussed further below.

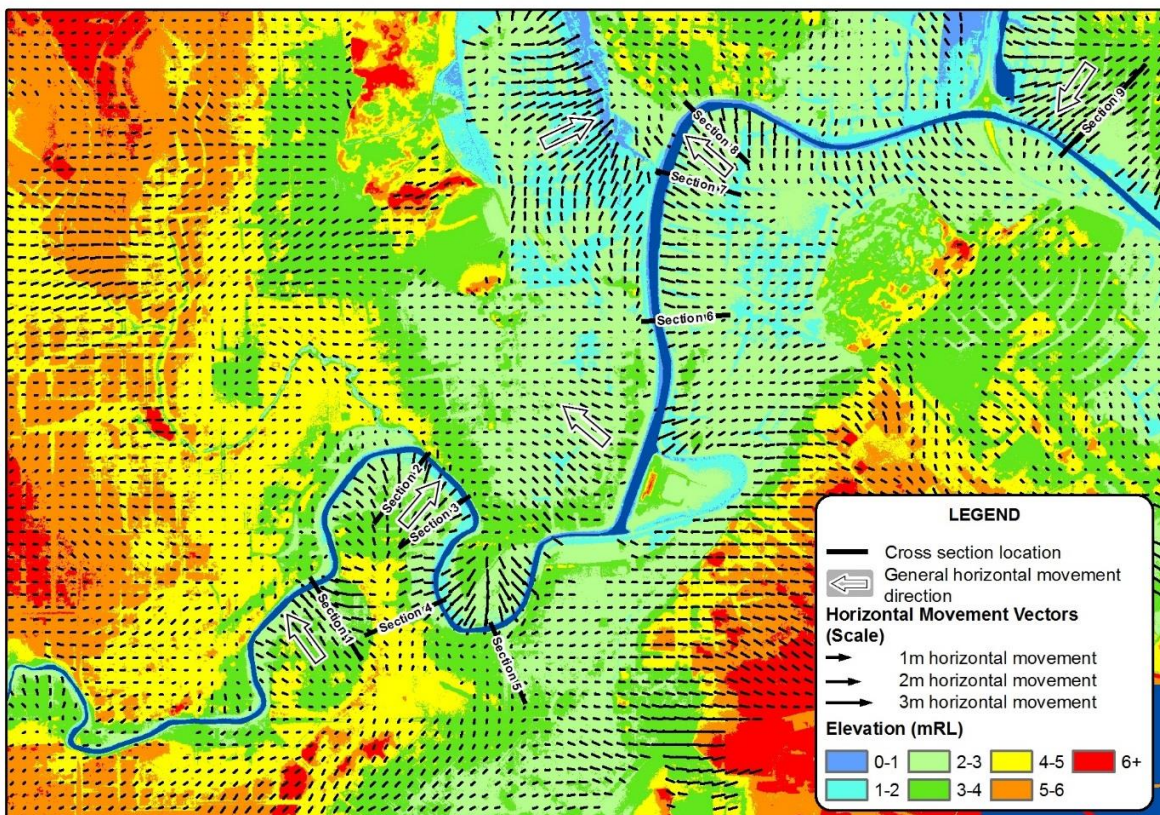


Figure F2.3: Ground surface elevation prior to the CES with LiDAR derived liquefaction related horizontal movement vectors overlaid.

The estimated horizontal movement vectors shown on Figure F2.3 are derived from LiDAR survey data that was obtained pre and post-CES. They represent the estimated liquefaction related horizontal movement as a result of the CES, calculated by taking the estimated total horizontal movement and subtracting the estimated tectonic horizontal movement.

The horizontal movement vectors are generated using a sub-pixel correlation method developed by Imagin' Labs Corporation and the California Institute of Technology (Beavan et al., 2011). The horizontal movement estimates were generated at an 8m grid spacing in most areas with LiDAR survey coverage, but are shown in Figures F2.3, F2.4 and F2.5 at a 56m grid spacing for presentation purposes.

The accuracy of the LiDAR derived horizontal movement is generally half of the accuracy of the vertical movement estimates (which is approximately $\pm 0.2\text{m}$ for 90 to 95% of the LiDAR survey area). This means the LiDAR derived horizontal movement accuracy is approximately $\pm 0.4\text{m}$ for 90 to 95% of the LiDAR survey area.

Comparison of the ground surface elevation and the liquefaction related horizontal movement vectors shows that lateral spreading tends to occur in a downslope direction (i.e. from higher elevation areas to lower elevation areas). It is noted that the slopes in the study areas which have large horizontal movements have relatively gentle slopes typically in the order of 1 to 2%. This is typical of most of the land affected by liquefaction related land damage in the Christchurch area. In most cases the direction of horizontal movement is towards a (i.e. the river banks). A notable exception in this study area is the horizontal movement to the north of the river between cross sections 5 and 6. This is indicating movement away from the river and towards a low point in this area and is attributable to the soils near the river bank having a higher resistance to liquefaction.

Figure F2.4 presents the same horizontal movement vectors as shown in Figure F2.3 overlaid onto the liquefaction related ground surface subsidence during the CES. The ground surface subsidence is derived by calculating the difference between the estimated total ground surface subsidence as a result of the CES³ and the estimated vertical tectonic movement.

Figure F2.4 demonstrates that significant ground surface subsidence (i.e. the red and pink areas) is generally associated with more significant lateral spreading zones (i.e. areas with larger horizontal movement vectors). As discussed in **Appendix A**, the ground surface subsidence is attributable to a combination of volumetric densification, volume loss due to liquefaction ejecta, localised topographic releveling and slumping associated with down slope lateral movement.

³ The estimated total ground surface subsidence is generated from LiDAR difference DEMs which are discussed in detail in **Appendix G**.

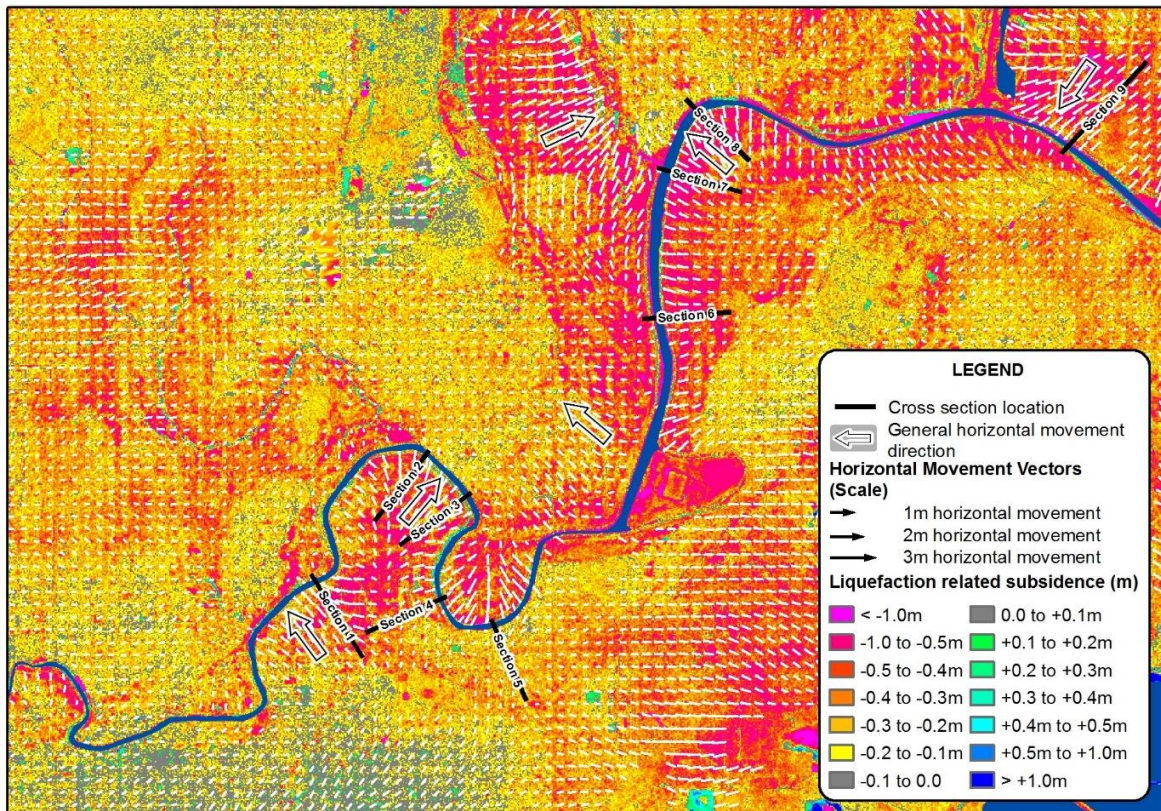


Figure F2.4: Liquefaction related ground surface subsidence during the CES with LiDAR derived horizontal movement vectors overlaid.

In addition to the horizontal movement estimates from the LiDAR surveys, independent methods that have been used to assess the severity, extent and direction of lateral spreading caused by the CES including estimation of horizontal movements derived from satellite imagery, GPS survey benchmarks, ground crack observation surveys (by summing up the crack widths along transects), land damage observations and river channel profile surveys. Each of these methods examines and measures different aspects of the lateral spreading caused by the CES as discussed below:

- **Satellite imagery** has been used to estimate the median horizontal movement for 8 x 8m cells within the Avon River area for the February 2011 earthquake (Martin & Rathje, 2014). The horizontal movement estimates derived from the satellite imagery are consistent with the estimated horizontal movements from the LiDAR surveys for the February 2011 earthquake. The difference between adjacent cells can be used to estimate the lateral stretching;
- **GPS surveys of benchmarks** provide an estimate of the horizontal movement at point locations. This method can only be used to estimate lateral spread at the GPS benchmark locations. They are typically not of sufficient density to assess the severity, extent and direction of the lateral spreading nor to estimate lateral stretch caused by the CES. Comparisons of the measured horizontal movement of the benchmark points for each of the main CES earthquakes show the measurements are consistent with the surrounding estimated horizontal movements from the LiDAR surveys and satellite imagery;
- **Ground crack (measurement) observation surveys** have been undertaken by Robinson et al. (2011, 2012 & 2013), Robinson (2015) and Cubrinovski & Robinson (2015) following the September 2010 and February 2011 earthquakes. These surveys estimate the lateral stretch along a transect as a summation of the observed crack widths. This is the conventional manner in which most lateral spread case histories were developed previously.

The results indicate that this survey method tends to under-estimate the total lateral movement relative to the other horizontal movement estimation methods. This is because absolute displacements are estimated from the LiDAR surveys whereas relative displacements (calculated from the cumulative sum of the crack widths) are relative to a reference point which is typically 150 to 200m away from the free-face. It is likely that for some of the ground crack surveys, the reference point along the transects has also moved, resulting in smaller displacements (since it assumes zero movement of the reference point) compared to the LiDAR surveys.

- **Land damage observations** based on property inspections are useful for understanding the spatial distribution of lateral spreading damage. While this data set does not provide an estimate of the magnitude of horizontal movement, it does map the areas visually affected by lateral spreading damage. The areas with the greatest horizontal movements (estimated from the LiDAR surveys and satellite imagery) for both the September 2010 and February 2011 earthquakes coincide with the mapped areas of lateral spreading damage (i.e. the severe and very severe land damage categories) as shown in Figure F2.5; and
- **River channel profiles** also provide an estimate of lateral spreading based on the relative movement of pre and post-CES river bank profiles. Figure F2.6 shows the pre and post-CES channel profiles in the locations shown on Figures F2.3 and F2.4. This method only provides an estimate of horizontal movement of the river bank which can be influenced by localised ground slumping of the river bank that can over-estimate the amount of horizontal movement relative to the other horizontal movement estimation methods.

Both the LiDAR and satellite imagery methods provide estimates of median horizontal movement for each 8 x 8m cell. Lateral stretch can be inferred from these survey methods as the difference between the horizontal movement estimates on two adjacent cells. However, in reality, the distribution of lateral spread is highly non-uniform and larger concentrations of lateral stretch occur at discrete locations (typified by ground cracks). Therefore, the LiDAR and satellite imagery methods are more useful for understanding the patterns and extent of horizontal movement rather than precise measurements of lateral spread.

The GPS surveys of benchmarks provide the most precise measurement of lateral spread at point locations but are typically collected at insufficient density to provide any meaningful interpretation of lateral spread patterns, nor the assessment of lateral stretching. Therefore, this method is only useful for understanding the accuracy and limitations of the other survey methods. Similarly, the ground crack (measurement) observation surveys do not capture all of the accumulated lateral stretch and the river channel profile methods often incorporate localised river bank slumping. As such, in isolation, none of the survey methods used to estimate the lateral spreading caused by the CES provide a complete picture and hence each the methods should be considered in conjunction with one another.

Based on analysis and examination of each of these data sets it can be seen that they are complimentary and largely consistent with one another in assessing the lateral spread which occurred in the Christchurch area as a result of the CES.

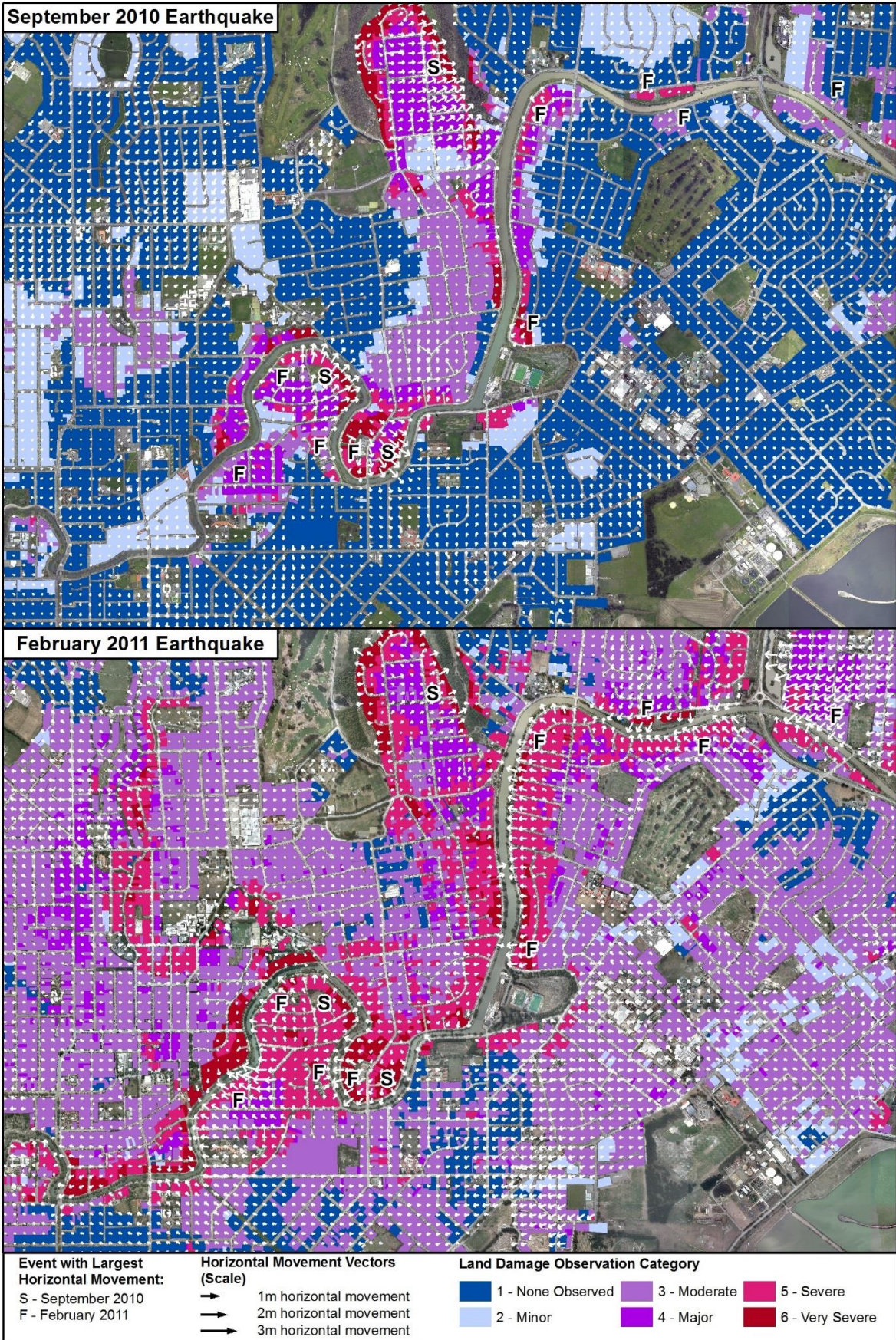


Figure F2.5: Land damage observations with LiDAR derived horizontal movement vectors overlaid for the September 2010 and February 2011 earthquakes.

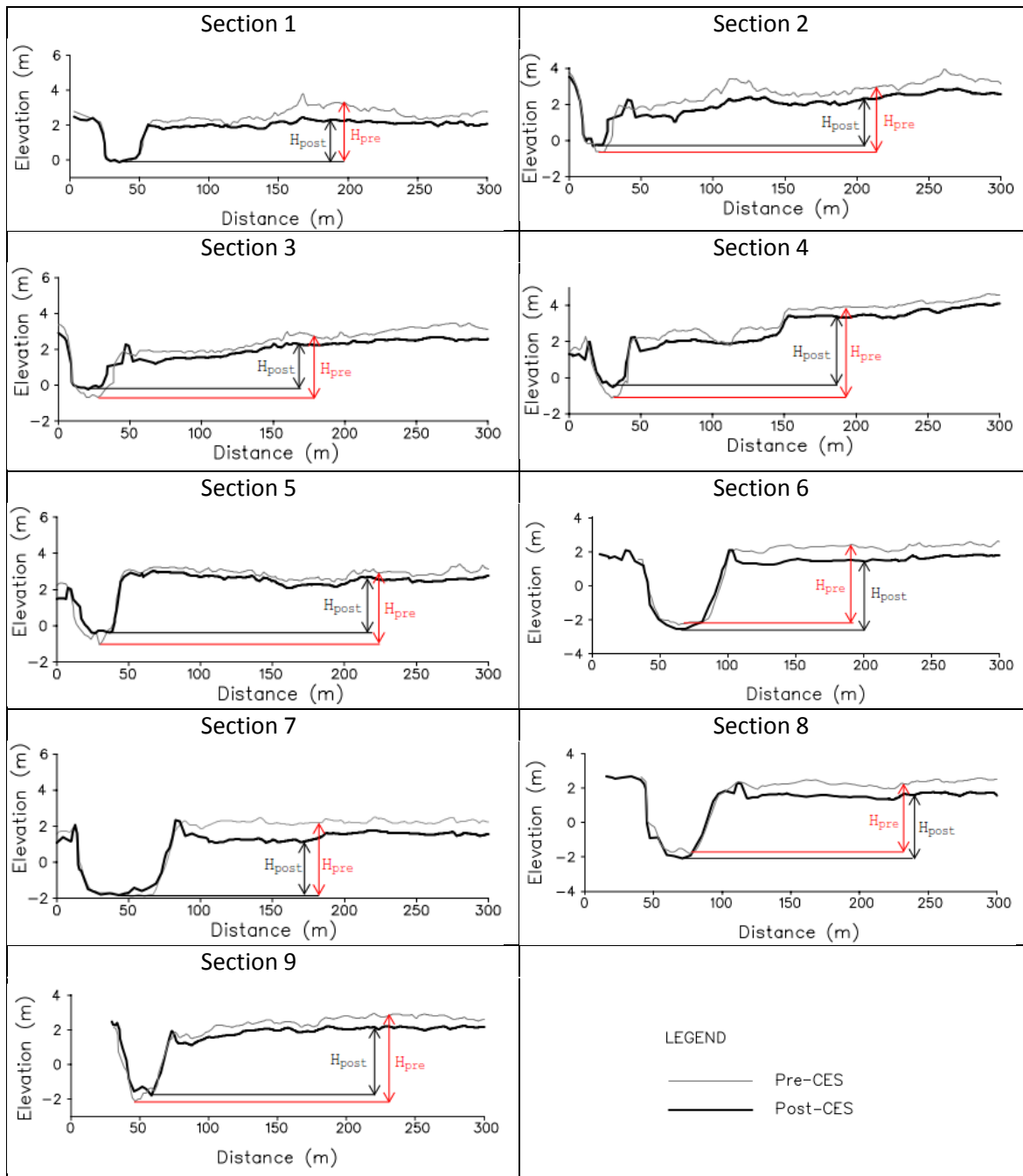


Figure F2.6: Pre and post-CES river and floodplain cross sections derived from a combination of direct river invert cross section survey measurements and LiDAR data. Cross section locations are shown on Figures F2.3 and F2.4.

Where the land is relatively flat, ground extension due to lateral spreading tends to extend a long way from the free-face (up to 400m in some areas as a result of the CES as shown by the horizontal movement vectors in Figures F3.3, F3.4 and F3.5). The horizontal ground movement accumulates over many sets of parallel cracks, so the land can be conceptualised as a series of blocks moving different distances, as shown in Figure F2.1. This geometry of lateral spreading tended to include large lengths of riverbank within the one block of ground movement (typically 0.5 - 2 km along the length of riverbank).

Geotechnical engineers and engineering geologists working in the field during the CES observed that the horizontal movements associated with lateral spreading in the Christchurch areas

initiated after the earthquake shaking had finished (i.e. they occurred post-seismically). In some instances these horizontal movements were continuing up to fifteen minutes after the earthquake shaking finished.

F3 The Effect of the CES on Lateral Spreading Vulnerability

F3.1 Lateral Spread Assessment Methods

As discussed in Section F2 liquefaction related lateral spreading is a highly complex process which is dependent upon a number of variables such as:

- The elevation difference between the base of the free-face (i.e., a road cutting, old terrace or a river bank) and the elevation of the land at the point of interest (referred to as the free-face height (H) from herein);
- The distance (L) from the base of the free-face to the point of interest;
- The earthquake ground motions including Peak Ground Accelerations (PGA) and earthquake magnitude (M_w);
- The thickness, relative density and location of liquefying layers within the soil profile; and
- Additional topographic and geological boundary conditions.

This complexity means that the development of lateral spreading assessment methods is particularly challenging and there are limitations associated with the methods that are currently available. It is important to understand these limitations and the degree of accuracy associated with the results from the methods.

The methods currently recommended for use in engineering practice in New Zealand (NZTA, 2014; NZGS, 2010) for the assessment of liquefaction related lateral spreading can be broadly categorised into the following two groups:

- Empirically based methods e.g. Youd et al. (2002) and Tokimatsu & Asaka (1998); and
- Newmark sliding block methods e.g. Jibson (2007) and Ambraseys & Srbulov (1995).

Other widely used methods are published in Saygili & Rathje (2008), Bray & Travararou (2007), Zhang et al. (2004), Makdisi & Seed (1978) and Seed & Martin (1966).

The methods and their key limitations are discussed under the subheadings that follow.

F3.1.1 Empirically Based Methods

Empirically based methods for the assessment of liquefaction related lateral spreading predict horizontal movement as a function of ground motion, geometry (i.e. H and L) and the liquefying soil layer parameters. These methods are derived from field observations and in-situ geotechnical investigation data. The three empirical methods listed above were developed by Tokimatsu & Asaka (1998), Youd et al. (2002) and Zhang et al. (2004). The two most recent methods are discussed below.

Youd et al. (2002) used multiple linear regression to analyse earthquake ground motion parameters, geometry and soil characteristics to develop an empirical relationship to predict horizontal movement associated with lateral spreading. The Youd (2002) model for displacement for free-face conditions is:

$$\log D_H = -16.713 + 1.532M - 1.406\log R^* - 0.012R + 0.592\log W + 0.540\log T_{15} + 3.413\log(100 - F_{15}) - 0.795\log(D_{50_{15}} + 0.1\text{mm})$$

where D_H is the horizontal movement in metres and W is the free-face ratio in percent and is equal to $100(H/L)$. The other variables in the equation are related to ground motion parameters

(M is the earthquake magnitude and R is the distance from the earthquake epicentre in km) and soil parameters (T_{15} is the thickness of the liquefying soil layer in m, F_{15} is the fines content of the T_{15} layer in percent and D_{50} is the median sediment grain size by weight of the T_{15} layer in mm). These parameters can be derived from seismic hazard studies and geotechnical investigations respectively.

The Zhang et al. (2004) method is derived from an estimate of the induced cyclic shear stress (estimated from CPT or SPT data) which is then empirically corrected for geometric effects such as H and L. The Zhang model for free-face conditions is as follows:

$$LD = 6 \left(\frac{L}{H} \right)^{-0.8} LDI$$

where LD is horizontal movement in meters and LDI is the lateral displacement index (an empirical approximation of the magnitude of cyclic shear stress) and is calculated by:

$$LDI = \int_0^{z_{max}} \gamma_{max} dz$$

where z_{max} = is typically taken as 2H and γ_{max} = maximum cyclic shear strain which is derived from liquefaction triggering assessments (refer to **Appendix A**) coupled with the Zhang et al (2004) maximum cyclic shear strain empirical equations.

The following are some of the key limitations associated with using empirically based methods for the assessment of lateral spreading:

- These empirical correlations are based on a limited case history database of lateral spreading observations. In particular, the CPT case history database is limited. The Youd (2002) model is based on SPT data only and modifications are required to use CPT data. The Zhang (2004) model is based on only 6 CPT case history sites; and
- Back analysis of observations of lateral spreading from the CES have demonstrated significant differences between the observed and the predicted horizontal movements using empirical methods.

The results from back analysis of the Youd (2002) model are variable. Robinson et al. (2013) and Bowen et al (2012) concluded that the model was significantly over-predicting, whereas Deterling (2015) concluded that the model was significantly under-predicting. It is noted that these studies were undertaken at different river cross-sections in different locations throughout Christchurch with different geological characteristics.

The results from the back analysis of the Zhang (2004) method are also variable. Deterling (2015) found that back analysis of the Zhang (2004) model indicates that predicted horizontal movements are within the same order of magnitude as those observed for sites within the specified range of L/H between 4 and 40 and that generally the Zhang (2004) model is an improvement over other models that were back analysed (such as Youd et al. (2002)). However, for L/H values less than 10, the Zhang model tended to under-predict displacements. Conversely, Robinson (2015) found that back analysis of the Zhang (2004) model resulted in relatively poor correlation with the observed horizontal movements.

F3.1.2 Newmark Sliding Block Methods

Newmark sliding block methods model land movement as a block of soil that slides on a defined failure surface when subjected to ground motions that approximate those experienced during an earthquake. The land movement is estimated by integrating acceleration (a) twice with respect to time over the parts of an earthquake acceleration-time history which initially exceed the minimum yield acceleration (a_{yield}) required to initiate sliding by overcoming the friction resistance

between the block and the failure surface it slides on until the velocities of the sliding block and underlying ground coincide.

There are a number of different approaches that have been developed to apply the Newmark sliding block method. These methods can be used to estimate horizontal movement due to liquefaction induced lateral spreading due to inertial loading. The following are some of the key limitations associated with using a Newmark-based method for the assessment of lateral spreading:

- It was developed using seismic landslide case history and not liquefaction related lateral spreading case histories. Therefore its use in the assessment of lateral spreading is beyond the scope of the original research; and
- The Newmark based methods all assume an inertial mechanism causing the lateral spreading that is inconsistent with the post-seismic observations of liquefaction related lateral spreading that were made during the CES (i.e. the lateral spreading occurred after the earthquake shaking had stopped as discussed in Section F2).

F3.1.3 Application of Lateral Spread Assessment Methods to the CES

The limitations and variability of both the empirically based and the Newmark sliding block methods mean that they are not ideal tools to assess lateral spreading vulnerability throughout Christchurch. However, the empirically based methods are still useful to gain insight into the factors that influence lateral spread.

Inspection of the equations shows that the empirically based methods are in the general form:

$$\text{Lateral movement} = \text{function of } \left(\frac{H}{L}, \text{ground motion parameters and soil properties}\right)^4$$

As discussed in Section 6.3, the 100 year return period ground motions are assumed to be a constant when assessing the change in liquefaction vulnerability as a result of ground surface subsidence from the CES. Similarly as discussed in Section 6.5, the soil properties in the Christchurch area have not changed as a result of the CES. **Appendix E** provides copies of CPT pairs that were pushed pre and post-CES.

Therefore, the primary influence on the estimate of horizontal movement that has changed as a result of the CES is the H/L ratio which has decreased (because the free-face height has decreased as a result of the CES as discussed below). Therefore, the amount of future estimated horizontal movement is also expected to decrease for the same level of earthquake shaking.

Similarly, for the Newmark sliding block methods the a_{yield} increases as a result of decreasing free-face height. This is because the flatter a slope has a smaller driving force requirement to induce lateral spreading.

While the LiDAR survey data demonstrates that the ground surface has subsided, the river channels have not subsided, and in most locations the river bed is now at higher elevations than it was prior to the CES due to lateral spreading and sedimentation from liquefaction ejecta entering waterways (Hughes et al., 2015).

Figure F2.6 shows the pre and post-CES river and floodplain cross sections. These cross sections are derived from a combination of direct river invert cross section survey measurements commissioned by the Christchurch City Council and LiDAR data available on the Canterbury

⁴ Note that the Zhang model is presented as $(L/H)^{-0.8}$ which is equal to $(H/L)^{0.8}$

Geotechnical Database. As indicated on the cross sections in Figure F2.6, the raising of the river bed and the subsidence of the surrounding flood plain has resulted in all cases in a decrease in the free-face height (H) at all cross section locations (i.e. $H_{\text{post}} < H_{\text{pre}}$).

The river cross section survey was undertaken in 2008, March 2011 (i.e. following the February 2011 earthquake) and in September 2011 (i.e. following the June 2011 earthquake). These surveys indicated that the June 2011 earthquake resulted in very minor changes to the river channel relative to the changes caused by the September 2010 and February 2011 earthquakes.

The river channel was not surveyed following the December 2011 earthquake on the basis that the June 2011 earthquake had not significantly changed the river channel. Also, the LiDAR survey data indicate that even less horizontal movement occurred in the December 2011 earthquake relative to the June 2011 earthquake. Therefore, while the river cross-sections in Figure F2.6 do not include changes due to the December earthquake, these changes are likely to be very small and hence the September 2011 river channel shape is a reasonable representation of the post-CES river channel.

In summary, the methods currently recommended for use in engineering practice for the assessment of liquefaction related lateral spreading all indicate an inverse relationship between the elevation difference between the base of the free-face and the elevation of the land at the point of interest, if all other parameters are held constant. The elevation difference between the base of the free-face and the elevation of the land at the point of interest has decreased due to ground surface subsidence and lateral spreading caused by the CES. Accordingly, on the basis that the soil properties have not changed (refer to Section 6.5 and **Appendix E**), the potential for horizontal movement due to lateral spreading has not increased over the CES (and in most cases decreased) for a given set of earthquake ground motions.

F3.2 Observed Horizontal Movements for each of the Main CES Earthquakes

Another means to investigate effect of changes to the land as a result of the CES on the vulnerability to lateral spreading in the Christchurch area is to analyse and track the estimated liquefaction related horizontal movements for each of the main earthquakes from the various lateral spreading measurement and observation methods listed in Section F2.2.

The ground crack (measurement) observation surveys undertaken by Robinson (2015) show that repeat measurements of horizontal movements at cross section transects in the Avonside and Dallington areas (marked with an “S” on Figure F2.5) were larger in the September 2010 earthquake compared to the February 2011 earthquake, even though the seismic demand was higher in the February 2011 earthquake.

Based on the examination of the Cone Penetration Test (CPT) data in these areas, the September 2010 earthquake provided sufficient seismic demand to liquefy the full soil profile in this area. Therefore, even though the seismic demand in the February 2011 earthquake was higher, the extent and thickness of liquefied soil is likely to have been similar for both earthquakes (as indicated in Figure 2.5). This indicates that the reduction in the lateral spreading in these areas for the February 2011 earthquake relative to the September 2010 earthquake is attributable to the reduction in the free-face height as a result of lateral spreading from the September 2010 earthquake (refer to Figures F2.5 and F2.6).

Conversely, in most other areas adjacent to the Avon River and its tributary streams, repeat lateral spread measurements presented in Robinson (2015) show that the measured horizontal movement for the February 2011 earthquake was larger than the measured horizontal movement for the September 2010 earthquake. These areas are marked with an “F” on Figure F2.5. This is primarily attributable to the larger seismic demand from the February 2011 earthquake triggering

a greater thickness and extent of liquefying soils (based on examination of the CPT in these areas) resulting in a greater potential for lateral spreading to occur (as indicated in Figure 2.5 by visually comparing the mapped liquefaction related land damage extents in the September 2010 and February 2011 earthquakes). While the horizontal movements were generally larger in the February 2011 earthquake, when considered relative to the seismic demand, the horizontal movements were generally similar to or smaller than the September 2010 earthquake.

The horizontal movement estimates derived from the LiDAR survey data for the September 2010 and February 2011 earthquakes are consistent with the ground crack (measurement) observation surveys undertaken by Robinson (2015).

Bouziou (2015) undertook spatial statistical analysis on the liquefaction related horizontal movement vectors derived from the LiDAR surveys (shown in Figures F2.2 and F2.3) for the September 2010, February 2011 and June 2011 earthquakes. For this study Bouziou (2015) selected a subset of the LiDAR data and removed areas that contribute to LiDAR error such as densely vegetated zones and areas with multi-storey building damage. In this work, Bouziou (2015) demonstrated that over the assessment area, on average, the most severe liquefaction related horizontal movement occurred in the September 2010 earthquake and reduced in subsequent earthquakes.

To further examine the spatial analyses, the work undertaken by Bouziou (2015) has been expanded upon by:

- Inclusion of the estimates of liquefaction related horizontal movements during the December 2011 earthquake;
- Further refinement of the study area through the removal of additional areas with erroneous data in parks and rivers where reliable estimates of the horizontal movements from the LiDAR surveys cannot be made; and
- Sub-categorisation of the horizontal movement for the various mapped land damage observation categories for each of the main CES earthquakes during the CES as shown in Table B.2 in **Appendix B**, Figure F2.5 and Figures K1.5 to K1.8 in **Appendix K**.

The refined study area is presented in Figure F3.1. Areas in blue show the common area where LiDAR surveys were undertaken after each of the main earthquakes during the CES. Areas in red were eliminated from the study by Bouziou (2015) to remove the areas with erroneous data. The areas in orange are the additional areas where erroneous data that have been eliminated for the horizontal movement analysis presented in this section.

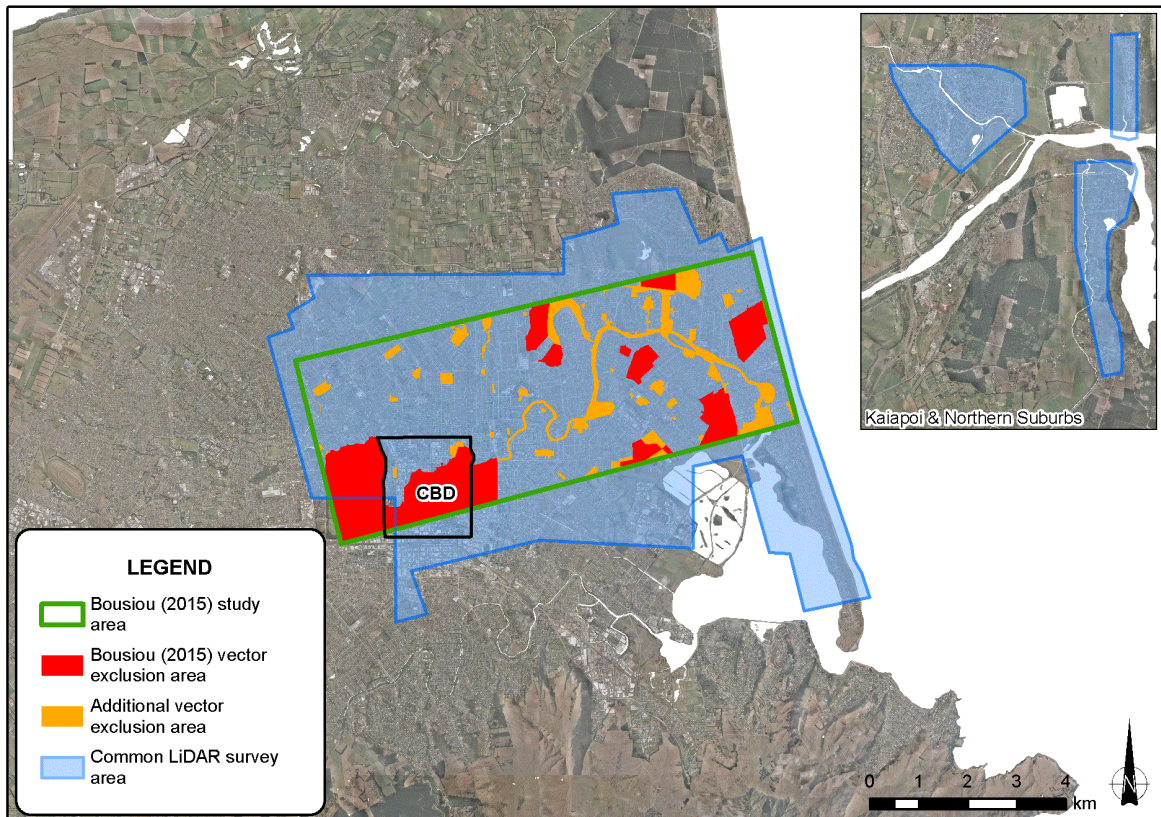


Figure F3.1: Study area and the areas where erroneous LiDAR derived horizontal movement data was excluded, superimposed on the common area of the LiDAR for the September 2010, February 2011, June 2011 and December 2011 earthquakes.

As discussed in Section 5.8, land damage observations for each of the four main earthquakes during the CES were recorded as one of six different land damage severity categories. The six land damage severity categories with a brief description of the types of land damage they represent are provided in Table B.2 in **Appendix B**.

Figure F3.2 shows the cumulative frequency distributions of the liquefaction related horizontal movement of the study area shown in Figure F3.1 for the six land damage severity categories for the four main earthquakes in the CES as shown in Figures K1.5 to K1.8 in **Appendix K**. The “none observed”, “minor” and “moderate” land damage categories include properties which sustained “no apparent lateral movement” based on ground and aerial photo mapping for that earthquake.

While the “major” land damage category is described as having “limited visual evidence of lateral movement” (refer to Table B.2 in **Appendix B**) it is possible that these properties have sustained horizontal movement due to stretching of the land or block movement that was not visually apparent on an individual property basis. This is primarily because a lot of these properties were covered with liquefaction ejecta which made it difficult to see the underlying evidence of any ground cracking and/or lateral stretching. The “severe” and “very severe” land damage categories include properties mapped with moderate to extensive lateral spreading.

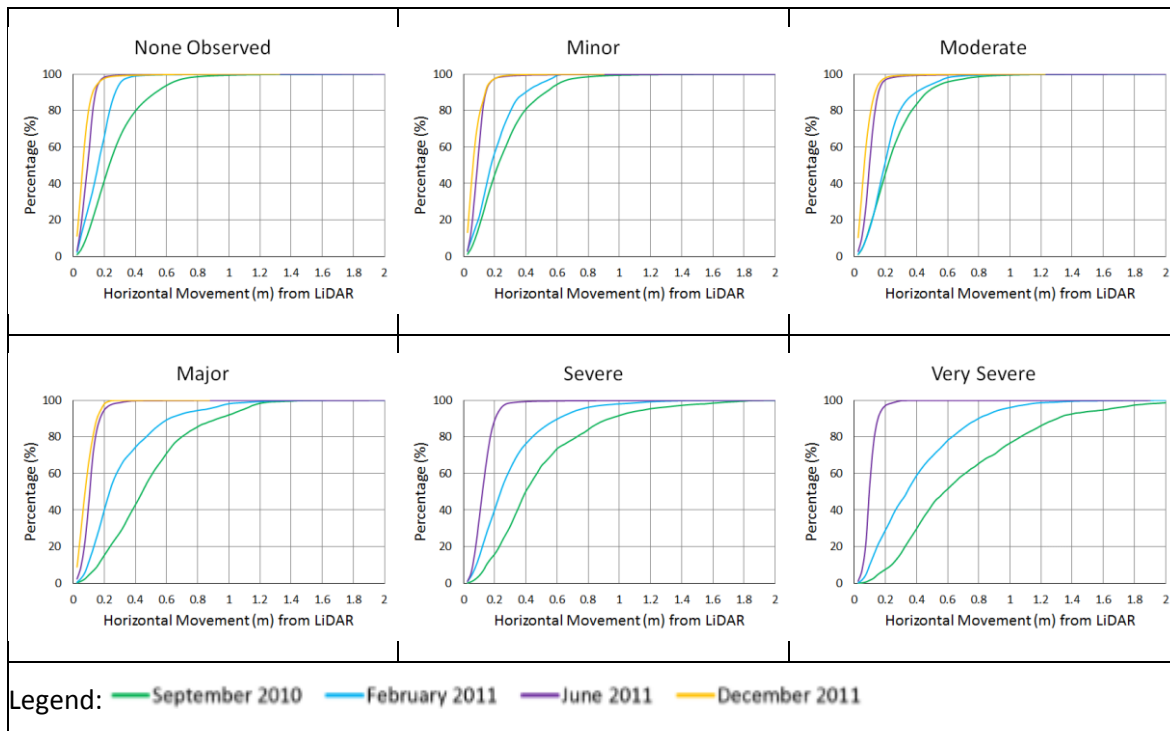


Figure F3.2: Plots showing the cumulative frequency distribution of the estimated liquefaction related horizontal movement for the six land damage observation categories during the four main earthquakes in the CES.

Figure F3.2 shows that the amount of liquefaction related horizontal movement increases with increasing mapped land damage severity.

The population of properties which sustained “none observed”, “minor and “moderate” land damage have very similar cumulative frequency distributions of liquefaction related horizontal movement. For each of the four main earthquakes, 80% of the properties moved less than 0.4m (i.e. within the accuracy limits for 95% of the LiDAR survey area).

The population of properties that sustained “major”, “severe” and “very severe” land damage show that in the September 2010 and February 2011 earthquakes more horizontal movement occurred compared to the June 2011 and December 2011 earthquakes. The most severe horizontal movement occurred on those properties which sustained “very severe” mapped land damage. This was less than 1m for 80% of the properties mapped with this type of land damage following the September 2010 earthquake and less than 0.6m for 80% of the properties mapped with this type of land damage following the February 2011 earthquake.

While for all land damage severity categories the typical liquefaction related horizontal movements were largest in September 2010, smaller in February 2011 and smaller again in the June 2011 and December 2011 earthquakes, care should be taken in appropriately interpreting the results presented in Figure E3.2. As discussed earlier, the lateral spreading in many areas increased in the February 2011 earthquake compared to the September earthquake, due to the higher seismic demand. While the typical horizontal movements for each land damage category decreased, many of the properties which were mapped as a less severe land damage category changed to a more severe category following the February 2010 earthquake, making comparisons between events difficult to interpret.

Therefore, further analyses were undertaken on the horizontal movements on the subset of 1,200 properties categorised as sustaining “severe” or “very severe” land damage during the September 2010 earthquake and again in the February 2011 earthquake (i.e. the areas marked with “S” on

Figure E2.5). The cumulative frequency distributions of horizontal movements for these 1,200 properties for the September 2010, February 2011, June 2011 and December 2011 earthquakes are shown in Figure E3.3. This figure demonstrates that properties, which sustained lateral spreading in the September 2010 earthquake (most of which are in the areas marked “S” on Figure E2.5), have statistically moved less horizontally in each subsequent earthquake. This conclusion is consistent with the lateral spreading crack measurement surveys made by Robinson (2015) and is also consistent with the cross section data shown in Figure F2.6. This Figure shows a reduction in H progressively through the CES as a result of ground surface subsidence reducing the potential for horizontal movements to occur.

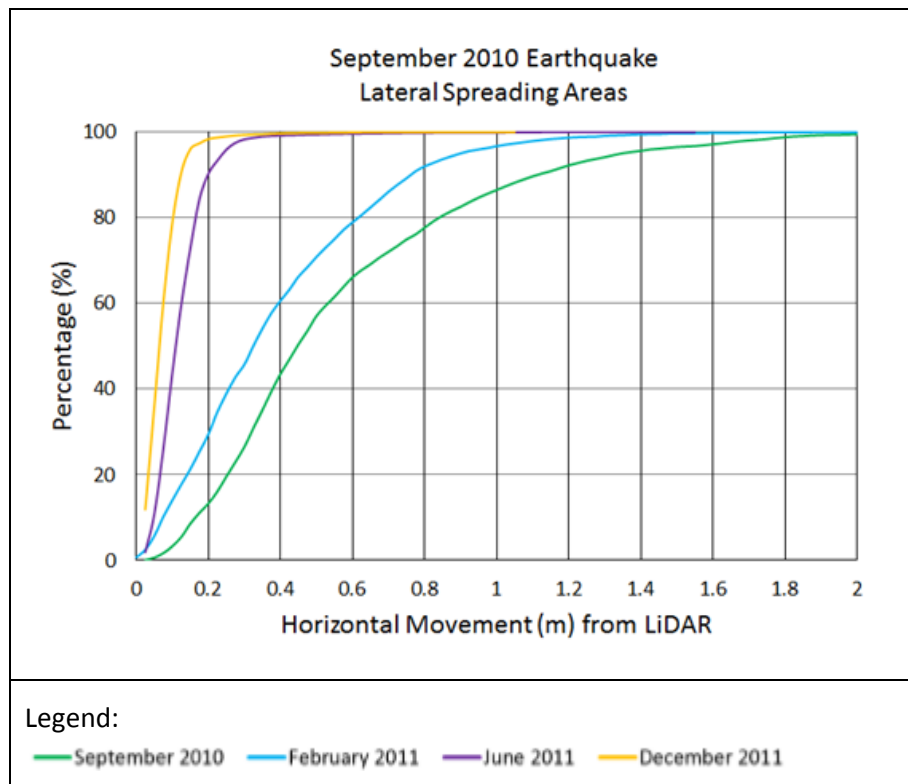


Figure F3.3: Cumulative frequency distribution for properties categorised as sustaining “severe” or “very severe” land damage observation categories for each of the four main CES earthquakes.

F3.3 Conclusion

On the basis that the elevation difference between the base of the free-face and the elevation of the land at the point of interest has remained the same or reduced as a result of ground surface subsidence and lateral spreading caused by the CES, the potential for lateral spreading very likely has not increased and in most instances likely has decreased. This is supported by the liquefaction related horizontal movement estimates from the LiDAR surveys, satellite imagery, GPS based benchmark surveys, ground crack observation surveys (by summing up the crack widths along transects), land damage observations and river channel profile surveys following each of the four main CES earthquakes. These horizontal movements show a reduction in the amount of lateral spreading for each of the three main earthquakes subsequent to the September 2010 earthquake relative to the seismic demand for each earthquake.

F4 References

Ambraseys, N. & Srbulov, M. 1995. Earthquake induced displacements of slopes. *Soil Dynamics and Earthquake Engineering*, 14(1995): 59-71.

- Beavan, J. Levick, S., Lee, J. & Jones, K. 2012b. *Ground displacements and dilatational strains caused by the 2010 - 2011 Canterbury Earthquakes*. GNS Science (Consultancy report 2012/67). GNS Science, Lower Hutt.
- Bouziou, D. 2015. *Earthquake-Induced Ground Deformation Effects On Buried Pipelines*. Ph. D thesis, Ithaca: Cornell University.
- Bowen, H. J., Jacka, M. E., van Ballegooy, S. & Sinclair, T. J. E. 2012. Lateral spreading in the Canterbury earthquakes - Observations and empirical methods. *15th World Conference on Earthquake Engineering*, Lisbon.
- Bray, J.D. and Travasarou, T. 2007. Simplified procedure for estimating earthquake-induced deviatoric slope displacements, *Journal of Geotechnical and Geoenvironmental Engineering*, 133(4): 381-392.
- Cubrinovski, M. & Robinson, K. 2015. Lateral spreading: evidence and interpretation from the 2010-2011 Christchurch earthquakes, *6th International Conference on Earthquake Geotechnical Engineering*, Christchurch.
- Deterling, O. C. 2015. *Factors Influencing the Lateral Spread Displacement from the 2011 Christchurch, New Zealand Earthquake*. Masters thesis, Austin: The University of Texas.
- Hughes, M., Quigley, M., van Ballegooy, S., Deam, B., Bradley, B., Hart, D. & Measures, R. 2015. The sinking city: Earthquakes increase flood hazard in Christchurch, New Zealand. *GSA Today*, March/April 25(3): 4-10.
- Jibson, R. W. 2007. Regression models for estimating coseismic landslide displacement. *Engineering Geology*, 91(2007): 209-218.
- Makdisi, F.I. & Seed, H.B., 1978. Simplified procedure for estimating dam and embankment earthquake-induced deformations. *ASCE Journal of the Geotechnical Engineering Division* 104: 849-867.
- Martin, J. G. & Rathje, E. M. 2014. Lateral Spread Deformations from the 2011 Christchurch, New Zealand Earthquake Measured from Satellite Images and Optical Image Correlation. *10th National Conference in Earthquake Engineering*, Earthquake Engineering Research Institute (EERI), Anchorage, AK.
- Ministry of Business, Innovation and Employment (MBIE) 2012. *Repairing and rebuilding houses affected by the Canterbury earthquakes*. Ministry of Business, Innovation and Employment. Available from: <http://www.building.govt.nz/guidance-on-repairs-after-earthquake>
- New Zealand Geotechnical Society (NZGS) 2010. *Geotechnical earthquake engineering practice*,: New Zealand Geotechnical Society.
- New Zealand Transport Agency (NZTA) 2014. *Bridge manual (SP/M/022)*, New Zealand Transport Authority.
- Olson, S. M. & Johnson, C. I. 2008. Analyzing Liquefaction-Induced Lateral Spreads Using Strength Ratios. *Journal of Geotechnical and Geoenvironmental Engineering*, 134(2008): 1035 – 1049.
- Robinson, K., Cubrinovski, M. & Kailey, P. & Orense, R. 2011. Field Measurements of Lateral Spreading following the 2010 Darfield Earthquake. *The Ninth Pacific Conference on Earthquake Engineering*, Auckland, New Zealand.
- Robinson, K., Cubrinovski, M. & Bradley, B. A. 2012. Lateral Spreading Measurements from the 2010 Darfield and 2011 Christchurch Earthquakes. *Australia – New Zealand Conference on Geomechanics*, Melbourne, Victoria, Australia.

Robinson, K., Cubrinovski, M. & Bradley, B. A. 2013. Sensitivity of predicted liquefaction-induced lateral displacements from the 2010 Darfield and 2011 Christchurch Earthquakes. *Proceedings of the 2013 Technical Conference and AGM*, Wellington, New Zealand Society for Earthquake Engineering.

Robinson, K. 2015, *Liquefaction-induced lateral spreading in the 2010-2011 Canterbury Earthquakes*. Ph. D thesis, University of Canterbury.

Saygili, G. and Rathje, E.M. 2008. Empirical Predictive Models for Earthquake-Induced Sliding Displacements of Slopes, *Journal of Geotechnical and Geoenvironmental Engineering*, 134(6): 790-803.

Seed, H.B. & Martin, G.R., 1966. The seismic coefficient in earth dam design. *ASCE Journal of the Soil Mechanics and Foundations Division* 92: 25-58.

Tokimatsu, K. & Asaka, Y. 1998. Effects of liquefaction-induced ground displacements on pile performance in the 1995 Hyogoken-Nambu earthquake. *Soils and Foundations*, Special Issue No. 2: 163–177.

Varnes, D. J. 1978. Slope movement types and processes. *Landslides – Analysis : Special Report 176*, R. L. Schuster and R. J. Krizek, eds., Transportation Research Board, Washington D. C.

Youd, T. L., Hansen, C. M. & Bartlett, S. F. 2002. Revised multi-linear regression equations for prediction of lateral spread displacement. *Journal of Geotechnical and Geoenvironmental Engineering*, 12(128): 1007-1017.

Zhang, G., Robertson, P. K. & Brachman, R. W. I. 2004. Estimating Liquefaction-Induced Lateral Displacements Using the Standard Penetration Test of Cone Penetration Test. *Journal of Geotechnical and Geoenvironmental Engineering*, 8(130): 861-871.